Absolute Test of Quantum Electrodynamics for Helium-Like Vanadium

David Paterson[1], Christopher T. Chantler[1], Larry T. Hudson[2], F. G. Serpa[2], John D. Gillaspy[2], and Endre Takács[2]

[1] School of Physics, University of Melbourne, 3010, Australia
[2] National Institute of Standards and Technology, Gaithersburg, Maryland 20899, USA

Abstract. Absolute measurements of the energies of helium-like vanadium resonances on an electron beam ion trap (EBIT) are reported. The results agree with recent theoretical calculations and the experimental precision (27–40 ppm) lies at the same level as the current uncertainty in theory (0.1 eV). The measurements represent a 5.7%–8% determination of the quantum electrodynamics (QED) contribution to the transition energies and are the most precise measurements of the helium-like resonances in the $Z = 19$–31 range. These are the first precision X-ray measurements on the National Institute of Standards and Technology EBIT and strongly commend the EBIT as a new spectroscopic source for QED investigations.

1 Introduction

Theoretical calculations of two-electron ion energy levels have been the topic of much research since the discovery of quantum mechanics. The contribution of relativistic effects via the Dirac equation and QED contributions has been intensely studied in the last three decades [1]. Two-electron systems provide a test-bed for quantum electrodynamics and relativistic effects calculations, and also for many body formalisms [2].

Theoretical calculations of energy levels in helium-like ions using variational techniques, relativistic corrections and a $Z\alpha$ expansion in the unified approach were pioneered by Drake in 1979 and 1988 [3,4]. Since then there has been active research in the calculation of energy levels in helium-like ions using new techniques. Major progress in theoretical calculations of QED contributions has occurred in the last decade, particularly in developments avoiding the $Z\alpha$ expansion by using all-orders techniques [5,6,7,8]. Plante *et al.* [5] provide a recent review of calculations of the $n = 1$ and $n = 2$ states of helium-like ions and present relativistic all-order many-body calculations. Rigorous QED calculations for the helium iso-electronic sequence are possible [9].

To critically test QED contributions at the 10% or better level in medium Z ions requires an experimental precision of 10–30 ppm. In many cases experiments of sufficient precision have not been performed which could resolve the differences between theories [5,8]. Earlier theoretical work [4] claimed an uncertainty of 1 ppm due to uncalculated higher order terms. However, the discrepancy between current theories approaches 30 ppm in the $Z = 23$ region. Recent

work of Persson *et al.* [9] estimates their uncertainty to be of order 0.1 eV or 20 ppm of helium-like resonances in vanadium due to missing correlation effects in QED terms. This new value for the uncertainty of computations in this region of Z is consistent with the theoretical variation observed. Precise experimental calibration of helium-like resonances ($n = 2$ to $n = 1$ transitions) can probe these discrepancies and uncertainties. The QED contributions to helium-like resonances in vanadium are 480–550 ppm of transition energies [4]. The literature has suggested that across the $Z = 19$–26 range experimental determinations of the w transition are on average 60 ppm greater than theory [10,11]. We have made absolute measurements of the helium-like resonances in vanadium with an uncertainty of 27 ppm for the w line.

Most precision spectroscopy of medium Z ions has been conducted at accelerators or tokamak plasmas, but the recent development of the electron beam ion trap (EBIT) has offered a new spectroscopic source to experimenters. Our experimental method takes advantage of the Doppler free and relatively clean spectra produced by an EBIT and is coupled with an external calibration source to allow absolute measurement of highly charged ions. These are the first precision X-ray measurements conducted at the NIST EBIT [12].

2 Experiment

The experimental configuration is shown in Fig. 1. The EBIT uses an intense and mono-energetic electron beam which is magnetically confined to trap and ionize charged ions. Metal ion species such as vanadium are created by a metal vapour vacuum arc (MEVVA) and are sequentially ionized as they enter the trap region of the electron beam. The NIST EBIT and spectra are described in further detail elsewhere [13,14].

We employ a Johann spectrometer with a Ge(220) crystal ($2d = 4.0007$ Å) which has a useful wavelength range between 1.9 Å and 2.8 Å in first order. The radius of crystal curvature is 1.846 m and the resolving power ($\lambda/\Delta\lambda$) of the spectrometer in the wavelength region of investigation is 2000–2500. The spectrometer has a 'Seemann wedge' which can be lowered towards the crystal pole, reducing the effective crystal area and the X-ray throughput, but improving resolution. The detector is a two-dimensional position-sensitive proportional counter which employs capacitive charge division from a backgammon design cathode to determine position [15,16]. The spectrometer has a fixed crystal radius so the detector does not always remain on the Rowland circle. This has substantial systematic effects on measurements [17].

We locate the EBIT source and calibration source inside the Rowland circle by design. Bragg diffraction angles of calibration lines are in the range 29–45° while the helium-like resonances are observed around 39°. The plane of crystal dispersion is parallel to the electron beam axis. The crystal acts as a polarizer at Bragg angles near 45° and radiation polarised perpendicular to the electron beam axis is the dominant diffracted component.

2.1 Calibration

Calibration is a detailed and extensive procedure because we map the dispersion function of the spectrometer across a broad range of wavelengths around the region of interest. Using a large number of calibration lines ensures the dispersion function is well determined and a wide range of wavelengths ensures that any higher order wavelength dependent effects are included. We systematically investigate effects of variations of source size and Seemann wedge position during calibration. This is necessary for precise absolute measurement.

The calibration source consists of a 20 keV electron gun and a series of metal targets (Mn, Cr, V, Ti) located on the opposite port to the spectrometer as indicated in Fig. 1. Calibration spectra are collected for a range of $K\alpha$ and $K\beta$ characteristic wavelengths (1.9 Å–2.8 Å) about the helium-like resonances of vanadium. $K\alpha_1$ and $K\alpha_2$ are well resolved in our system and so the $K\alpha$ doublet provides two reference wavelengths at one detector location. This gives an absolute calibration of detector scale [17,18].

A solid state Si(Li) detector is used to maximise the flux of helium-like vanadium transitions, to minimise contamination from undesirable charge states and to monitor dielectronic recombination transitions. A small amount of pure nitrogen gas is leaked into the trap (injection pressure $\approx 5 \times 10^{-7}$ Torr) to increase the proportion of lower charge states via evaporative cooling.

In plasma experiments the electron energy distribution is very broad. By contrast, the electron beam energy distribution of the EBIT is narrow and the energy can be tuned. The helium-like resonances are isolated by setting the electron beam energy to 7.0 keV, 1.85 keV above the direct electron-impact exci-

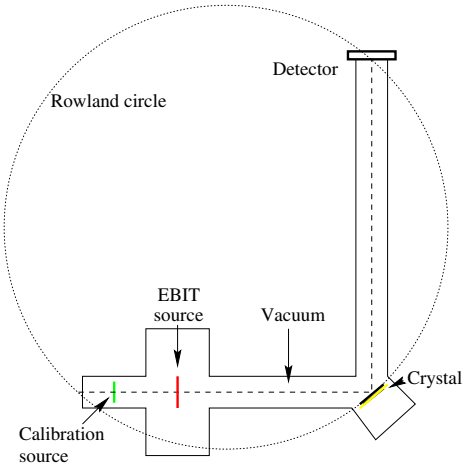

Fig. 1. Spectrometer configuration at NIST EBIT; note that the EBIT source is located well inside the Rowland circle. The spectrometer is in the "perpendicular" orientation where the axis of the spectrometer is perpendicular to the long axis of the EBIT source. The detector arm moves vertically with changes in diffraction angle.

tation energy. At this energy dielectronic resonances are not excited, resulting in a spectrum clean of dielectronic satellite lines. The space charge of the electron beam will alter the electron beam energy by approximately 100 eV from that due to the accelerating voltage. The electron beam current was typically 140 mA.

In the EBIT an axial trapping potential is created by a series of three drift tubes and the depth of the trap may be varied rapidly. The sequencing of each input of ions from the MEVVA with the lowering of the potential walls is important in maximising the number of trapped ions. The duration and height of trap formation is optimised to maximise trapped ions and to avoid the build up of undesirable metastable states and background barium ions. A single spectrum is collected and saved every 2 hours and spectra collected under identical conditions are summed during the data analysis. Fig. 2 shows a helium-like vanadium resonance spectrum from 24 hours observation, with the intensity and lithium-like resonance indicated.

2.2 Clinometry

During the relatively long observation periods any shifts in the diffraction angle or detector position must be monitored and minimised. Clinometers monitor the detector and crystal angles continuously with arcsecond resolution. Spectra were collected continuously for several days with 24 hour-a-day EBIT operation. Most observations were made with the Seemann wedge removed to maximise flux. The detector has a window wider than the full helium-like resonance spectrum of the EBIT. Hence several detector angles centering on various features of the spec-

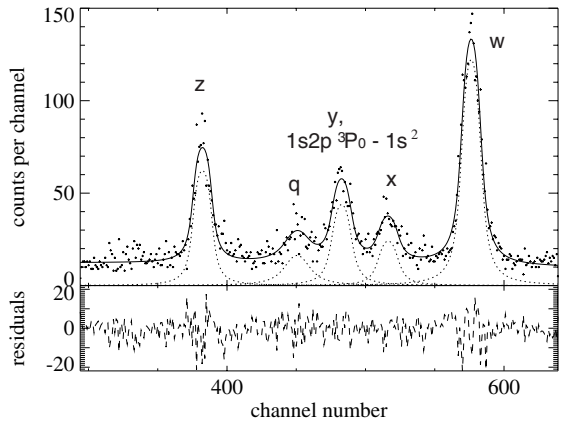

Fig. 2. Summed observations of helium-like vanadium spectra at the NIST EBIT representing some 24 hours of observation. The q ($1s2s2p\ ^2P_{3/2} \rightarrow 1s^2 2s\ ^2S_{1/2}$) contamination does not impair the final measurement. Spectra are fitted with Lorentzian convolved with slit profile and a background quadratic term. The dotted lines are the fitted profiles to each resonance line, the solid line is the sum of all fitted profiles and background

trum were able to investigate detector linearity. A post-measurement calibration ensured that no changes in alignment had occurred during the measurement.

3 Curved Crystal Theory and Systematic Shifts

Curved crystal geometries are often used in precision X-ray spectroscopy to obtain increased signal and lower statistical error or to focus an extended source. Dynamical X-ray diffraction plays a crucial role in any wavelength dispersive spectroscopy such as ours. The best known systematic shift in X-ray diffraction is the refractive index (RI) correction which is due to the mean change in refractive index in the crystal changing the angle of incidence relative to the air or vacuum. The angle of diffraction θ_B is shifted from that determined by Bragg's law of diffraction to become

$$n\lambda = 2d \sin\theta_B \left(1 - \frac{1 - \mathrm{RI}}{sin^2\theta_B}\right) \tag{1}$$

where RI is the index of refraction (specific to wavelength and the crystal). The magnitude of the refractive index correction is 100–300 ppm [19,20] depending upon the wavelength, crystal and geometry and so must be determined to a few percent.

Most curved and flat crystal spectrometry QED investigations have addressed systematic corrections based upon ray-tracing methods, incorporating the simple refractive index correction [21,22]. Some of these QED measurements were calibrated using wavelengths observed in different orders of diffraction [10]. These measurements, however, did not use a full dynamical diffraction theory to calculate systematic shifts and therefore did not consider additional significant shifts relating to depth penetration, lateral shifts, source size and detector location. Any of these effects can cause systematic shifts comparable to the refractive index correction. All systematic shifts down to the level of 10–30 ppm must be accounted for to perform useful tests of QED in medium Z highly charged ions. These issues led to the development of the first theory to combine curvature and mosaicity in a dynamical diffraction theory by Chantler [23,24].

3.1 Depth Penetration

Depth penetration refers to the mean depth that X-rays penetrate into the crystal and the effect that this penetration has upon the observed diffraction angle. For curved crystals depth penetration at angles other than normal to the surface will result in a variation of the angle of incidence in successively deeper crystal layers. The depth penetration of X-rays into a crystal can have effects larger than refractive index shifts [20]. It is the dominant systematic in many curved crystal measurements, and is independent of refractive index and ray-tracing (geometrical) corrections. The magnitude of this effect is dependent upon diffract ion order and angle of incidence. The resulting shift in angle for curved crystals

(radius $2R_z$ where R_z is the Rowland circle radius) can be estimated from the simple approximation

$$\Delta\theta_{\text{in/out}} \simeq \arccos\left[\left(1+\frac{\bar{d}}{2R_z}\right)\cos(\theta_B \pm \alpha_p)\right] - (\theta_B \pm \alpha_p) \qquad (2)$$

where $\bar{d}$ is the mean depth of penetration and α_p is the mean angle of diffracting planes to the crystal surface [20]. A rigorous calculation with 1% accuracy requires dynamical diffraction theory rather than such simple estimates. The strong dependence of this shift upon diffraction order, due to the dependence of attenuation (μ) upon energy, implies that any X-ray QED measurement employing diffraction in different orders should compute this explicitly.

3.2 Lateral Shifts

Lateral shifts are also due to depth penetration and refer to a shift in the exit location of an X-ray at the crystal surface. This results in a transverse shift at the detector, typically 10%–100% of refractive index corrections [20]. While ray-tracing can adequately describe geometrical effects outside the crystal, the effects of depth penetration and lateral shifts require full dynamical diffraction theory.

Estimates of shifts of spectra in curved crystal geometries are often calculated for an ideal detector located on the Rowland circle. However, the detection surface is usually flat and therefore cannot lie on the Rowland circle. Detectors located on a fixed length detector arm will additionally travel off the Rowland circle as the Bragg angle is scanned unless the crystal curvature is simultaneously scanned (which raises problems of stress hysteresis). Conventional shifts calculated for detection on the Rowland circle do *not* agree with shifts at a flat extended detector and this systematic error can be 100–200 ppm for any Johann curved crystal spectrometer. We have incorporated flat surface detectors located off the Rowland circle into the general theory [18,17].

4 Data Analysis and Error Sources

Calibration and EBIT spectra are fitted with Lorentzian convolved with slit profiles. The width of the Lorentzian and common slit components are free parameters in the fit. For calibration lines the background is negligible and not fitted. Helium-like resonances and the largest satellite are fitted with Lorentzian profiles convolved with slit profiles in addition to a constant background. Fig. 2 shows the result of profile fitting to a helium-like vanadium spectrum.

Reference wavelengths for calibration lines are corrected from Bearden's values [19] for the recent CODATA determination of lattice spacings and X-ray wavelengths [25]. The dispersion function is fitted to the 10 calibration wavelengths. The dispersion function relates the wavelength of a spectral feature located at the detector centre, to the angle of diffraction measured by clinometers.

The centroid of each clinometer distribution of an integrated spectrum gives the the crystal (θ_B) and detector ($2\theta_B$) angles. The dispersion function is determined by a bi-variate nonlinear least squares fit to the function

$$\Theta = \arcsin\left[\frac{DC - A(1)}{A(2)}\right] - \arcsin\left[\frac{CC - A(3)}{A(4)}\right] + A(0) \qquad (3)$$

where DC is the centroid of the detector clinometer, CC the centroid of the crystal clinometer, Θ the reference wavelength of the calibration line (adjusted for refractive index and all systematic corrections) and $A(0)$–$A(4)$ the parameters of the fit relating to offsets and scaling of clinometer response function, which is highly linear in $\sin\theta$.

One example of a systematic shift is that caused by the calibration source not being in the same location as the EBIT source. Our theoretical modelling determines the shifts of < 1 arcsecond associated with this mis-location. The dispersion function is not a simple relationship between angle and wavelength but a complex (but smooth) function of reference wavelengths, clinometer values, detector scale and systematic shifts.

4.1 Error Budget

The final error budget is laid out in Table 1. The statistical uncertainty varies between 9.5 ppm (w) and 31.0 ppm (x). The relatively low flux of the EBIT prohibits trivial improvement. The error is determined from curve fitting as the standard deviation of the centroid position for each resonance. This is consistent with a determination varying between 1/27 and 1/77 of the widths, which is a reasonable level of precision based on the statistics.

The uncertainty of the dispersion function determination reported in Table 1 is the estimated total uncertainty of the factors that contribute to the determination. The overall contribution of calibration source size and alignment uncertainty is 5 ppm. The statistical error associated with calibration lines is 2–3 ppm and the error associated with calibration profile fitting is < 5 ppm.

The major contribution to dispersion function uncertainty is the detector scale uncertainty at 15 ppm. This uncertainty relates to the absolute calibration of the detector position scale in channels per micron and the linearity of that scale. The helium-like resonances are widely spaced on our detector (w–z separation ≈ 8.5 mm) and uncertainty in the detector scale is critical when determining the position of these lines. The absolute detector scale is determined at $< 0.5\%$ which results in an average contribution to dispersion function imprecision of 15 ppm.

We have done explicit analysis to determine the error associated with the omission of the systematic shift caused by flat detector shape and location off the Rowland circle. This omission revealed a poor determination of the dispersion function and consequent errors of 100 ppm. Including this effect has allowed reduction of the dispersion function uncertainty to 20 ppm through the careful determination of systematic uncertainties.

Table 1. Error budget for helium-like vanadium measurement

Error source	Magnitude of error (ppm)			
	Resonance line			
	w	x	y	z
Statistical uncertainty of centroid position	9.5	31.0	22.3	12.9
Dispersion function determination[a]			19.6	
Reference wavelengths (Bearden [19])			12	
Diffraction theory[a]			6	
Temperature and diffraction crystal $2d$ spacing variation			< 5	
Doppler shifts			< 4	
Satellite contamination			< 4	
Total excluding statistics[b]			**24.9**	
Total	**26.7**	**39.8**	**33.4**	**28.1**

[a] Summation of related uncertainties (see text).
[b] Total excluding statistics: Sum of all errors except statistical uncertainty of helium-like vanadium observations.

Doppler shifts due to the low thermal velocities of the highly-charged ions in the EBIT are not significant sources of uncertainty. On average the Doppler shifts will be zero as there is no preferred direction of motion. Doppler broadening is 1.8 eV for 1 keV ions and we allow for a possible 1% asymmetry of velocity distribution resulting in a maximum Doppler shift of < 0.02 eV or < 4 ppm.

Summing all errors in quadrature results is a 27 ppm–40 ppm uncertainty. The main sources of uncertainty are therefore statistical, reference wavelengths and dispersion function determination. All major error sources are 'soft' and may be reduced further. Methods of reducing statistical uncertainty by improving spectrometer efficiency are being investigated and improved flux from the EBIT has been achieved in other studies [26].

5 Results and Discussion

Our results are the first absolute measurements of all the resonance lines in helium-like vanadium using an EBIT. We do not rely on a single calibration energy, but require a series of calibration lines to determine the dispersion function of the spectrometer. These measurements represent a 27 ppm–40 ppm determination of the helium-like resonance lines in vanadium. Results are summarized in Table 2 and the notation of Gabriel [27] for each transition is indicated.

Table 2. Energies of helium-like resonances in vanadium (V^{21+}), comparison to theory

Key	Transition	Theory [4]		NIST EBIT & Univ. Melbourne [12]		
		Energy (keV)	QED (ppm)	Energy (keV)	ΔE (ppm)	Test of QED (%)
w	$1s2p\ ^1P_1 \rightarrow 1s^2\ ^1S_0$	5.205 15	471.1	5.205 10(14)	−10.1	5.7%
x	$1s2p\ ^3P_2 \rightarrow 1s^2\ ^1S_0$	5.188 72	478.1	5.189 12(21)	80.1	8.4%
y	$1s2p\ ^3P_1 \rightarrow 1s^2\ ^1S_0$	5.180 31	482.5	5.180 22(17)[c]	−19.2	6.9%
z	$1s2s\ ^3S_1 \rightarrow 1s^2\ ^1S_0$	5.153 88	415.5	5.153 82(14)	−10.8	6.7%

[a] QED: QED contribution to transition energy using QED definitions of Drake [4].
[b] ΔE: Energy (Expt−Theory)/Theory in ppm.
[c] Unresolved blend of y and $1s2p\ ^3P_0 \rightarrow 1s^2\ ^1S_0$ transitions.

5.1 Comparison to Theory

Our results for all of the helium-like vanadium resonance lines are compared to the theory of Drake [4] in Table 2. The values for the w ($1s2s\ ^1P_1 \rightarrow 1s^2$) and z ($1s2s\ ^3S_1 \rightarrow 1s^2$) transitions lie just below theory but well within experimental uncertainty. The x ($1s2p\ ^3P_2 \rightarrow 1s^2$) transition is the least intense of the helium-like resonance lines, so the statistical uncertainty is larger. However the result for the x line is less than $2\,\sigma$ from theory [4] which is within reasonable statistical variation. The results for the y and $^3P_0$ transition have been discussed in detail elsewhere [12].

The uncertainty of theoretical calculations including the estimation of missing or uncalculated terms has been receiving increasing scrutiny as techniques have advanced. One of the most recent two-electron Lamb shift calculations by Persson *et al.* [9] estimates missing correlation effects in QED contributions at 0.1 eV for all elements or 20 ppm of transition energies in medium Z ions. In earlier work, Drake [4] claimed uncertainty for $Z = 23$ was < 0.005 eV or 1 ppm of helium-like resonance lines due to uncalculated higher order terms. Some of the latest theoretical calculations for the w transition in medium Z ions are summarized in Table 3.

The discrepancy between theories is indicated and the maximum discrepancy ranges from 23 ppm to 30 ppm for $Z = 18$–26 and differences are consistent. Our measurements are at this level of uncertainty. A further indication of the uncertainty or accuracy of theory can be gained by considering the two configuration interaction (CI) calculations of Cheng *et al.* [6,7]. The latest calculations for mid-Z helium-like ions [7] has resulted in new values which have shifted by up to 14 ppm from the earlier calculation [6]. The difference has been attributed to the exclusion of the Latter correction to the Dirac–Kohn–Sham potentials from which the QED corrections are evaluated. The new results are considered to be more reliable [7] and are in closer agreement to the unified calculation

of Drake [4]. The availability of new high precision EBIT measurements for medium Z helium-like ions [12] has been a major stimulation for theoretical re-evaluation of QED contributions.

Table 2 also shows the QED contributions to helium-like resonance lines in vanadium as determined by Drake. The QED contributions are also expressed as a proportion of the relevant transition in ppm. The level at which our measurements test these contributions is between 5.7% and 8%. The theoretical QED contributions include mass polarization and nuclear size effects but these contribute less than 1% to the total. If the QED contributions to the $2l$ states are assumed to be correct, then the $1s$ QED contribution is measured to 6%.

Our result for the w line in vanadium is within our experimental uncertainty of the theory of Drake [4] and Plante *et al.* [5]. We therefore find no evidence of the earlier reported trend that experimental values are greater than theory [10]. Our measurements are compared with other experiments in the context of medium Z X-ray measurements in the following discussion.

Table 3. Selected w ($1s2p\ ^1P_1 \rightarrow 1s^2$) transition energies (eV) for vanadium and surrounding medium Z ions

Z	Experiment (eV)	Ref.	Theoretical transition energies		Ref.			ΔTh[a] (ppm)	QED[b] (eV)	2e[c] (eV)
		[4]	[5]	[7]	[6]	[8]				
18	3139.553(38)	[33]	3139.577	3139.582	3139.617		3139.65	23	1.055	0.09
22	4749.74(17)	[10]	4749.63	4749.64	4749.65	4749.71		17		
23	5205.10(14)	[12]	5205.15	5205.16	5205.18				2.474	0.16
24	5682.32(40)	[10]	5682.05	5682.06	5682.08	5682.15		18		
26	6700.08(24)	[23]	6700.40	6700.43	6700.45	6700.54	6700.60	30		
32	10280.70(22)	[29]	10280.14	10280.19	10280.25	10280.39		24	7.674	0.40

[a] ΔTh: Maximum discrepancy between theories.
[b] QED: QED contribution to the ground state ($1s^2\ ^1S_0$) [4].
[c] 2e: Two electron QED contribution extrapolated (see text) [9].

5.2 Two-electron Lamb Shifts

The two-electron Lamb shift has been a topic of considerable interest recently following significant variation in the recent calculations of two-electron contributions to the ground state of medium and high Z helium-like ions [9,5,4]. The "two-electron Lamb shift" can be defined as the difference between the hydrogenic $1s_{1/2}$ Lamb shift and the QED contributions to the helium-like ground state ($1s^2\ ^1S_0$). The two-electron Lamb shift relates to the two electron radiative QED Feynman diagrams (vacuum polarization and self-energy) due to

interactions between the electrons[9]. Nonradiative two-electron QED (ladder and crossed-photon diagrams) are negligible for $Z \leq 32$. We have calculated the two-electron Lamb shift by subtracting the results of Johnson and Soff [28] for the hydrogenic $1s_{1/2}$ Lamb shift from the QED contributions to the helium-like ground state from Drake [4]. For $Z = 32$ (germanium) we obtain 0.31 eV which can be directly compared to the 0.4 eV result of Persson *et al.* [9]. For vanadium, the two-electron Lamb shift calculated in this manner is 0.15 eV or 29 ppm of the $1s2s\ ^1P_1 \rightarrow 1s^2$ transition energy. Two electron QED calculations for $Z < 32$ are not available from Persson *et al.*, so no direct comparison can be made with Drake's calculation for vanadium.

As a simple alternative calculation, we have estimated the two-electron Lamb shift for helium-like ions of Z less than 32 by extrapolating the results of Persson *et al.* for $Z = 32$–92 using a power law fit (2e QED $= aZ^b$). The Z power dependence is interestingly found to be $b \approx 2.5$. Derived results for $Z = 18$ and 23 are tabulated with Persson's result for $Z = 32$ in Table 3. Theory might expect a power law dependence of $b = 3$ as the two-electron contributions scale as Z^3. The result ($b \approx 2.5$) from the power law fit to the sum of all computed contributions is in reasonable agreement with the expected theoretical value. For vanadium the two-electron Lamb shift is 0.16 eV or 31 ppm, slightly larger than the experimental uncertainty of 0.14 eV of our measurements. The agreement between this result obtained from extrapolation of the results of Persson *et al.* and the value obtained by direct calculation from Johnson and Soff and Drake is excellent (0.01 eV difference). For $Z = 32$, where the comparison can be made directly without extrapolation, the difference is 0.09 eV, remarkably consistent with the uncertainty estimate (0.1 eV) of Persson *et al.* for contributions from missing correlation effects in QED. A significant improvement in experimental precision would provide a critical test of two-electron QED.

In terms of basic physical effects included, the calculations of Drake and of Persson *et al.* are equivalent up to all terms of order α^3 (assuming that the Many Body Perturbation Theory expansion has converged sufficiently well), and also terms of order $\alpha^4 Z^6$ and $\alpha^4 Z^5$. Any difference between the two calculations should therefore scale as $\alpha^4 Z^4$, at least through the intermediate range of Z.

Persson *et al.* states that the missing correlation effects in their two-electron QED calculations is estimated to be of the order of 0.1 eV for all elements. Formally this should only be only be applied to the range of elements $32 < Z < 92$. The associated uncertainties for $Z < 32$ are unknown, but could be expected to increase in this regime. In the calculations of Drake, the uncertainty due to relativistic correlation effects in QED scales as $\alpha^4 Z^4$. The sources of the uncertainty are quite different in the calculations of Drake, and of Persson *et al.*. The lowest order Lamb shift is of order $\alpha^3 Z^4$, and so the leading two-electron correction is of order $\alpha^3 Z^3$, i.e. smaller by a factor of $1/Z$. Higher order correlation effects contribute further terms of order $\alpha^3 Z^2$, $\alpha^3 Z$,.... In the calculations of Persson *et al.*, it is the uncertainty in these correlation corrections to the lowest order (in α) Lamb shift that accounts for their estimate of 0.1 eV for all elements. In contrast, the calculation of Drake accurately sums this entire series of

terms, but there are relativistic correlation corrections to the QED shift of order $\alpha^4 Z^4$, $\alpha^5 Z^5$, ..., not included in his calculation. This accounts for Drake's error estimate of $1.2(Z/10)^4$ cm-1[4], scaling as Z^4.

In summary, the calculation of Drake accurately treats the $1/Z$ expansion of the nonrelativistic two-electron QED shift, but not the αZ expansion of relativistic and correlation corrections. The calculation of Persson *et al.* is improved for the αZ expansion, but not the $1/Z$ expansion of the nonrelativistic correlation terms. For larger Z the calculations of Persson *et al.* may be preferred, and for smaller Z the calculations of Drake may be preferable.

Measuring the helium-like $n = 2$ to $n = 1$ transitions can be sensitive to the excited state QED contributions if the precision is sufficient. The QED contribution to the $1s2s\ ^3S_1$ is 0.333 eV from Drake [4] or 65 ppm of the transition energy. Our measurement of the z ($1s2s\ ^3S_1 \rightarrow 1s^2$) transition is sensitive to the $1s2s\ ^3S_1$ QED contribution at the 40% level. Most previous experiments in the medium Z region have only measured the w transition, while others have only measured the w and close lying x and y lines. Ours is one of the most precise measurements of the z transition in medium Z ions.

Of course, the result is a direct measure of the $1s2s\ ^3S_1 \rightarrow 1s^2$ QED contribution. Most such measurements are insensitive to the excited state ($2s$ or $2p$) QED contribution. However, our measurement is indeed sensitive to the excited state QED contribution at the 40% level. Our result is comparable to the 51 ppm measurement for $Z = 32$ [29] which tests the $1s2s\ ^3S_1$ QED contribution at the 48% level.

5.3 Previous Helium-like Vanadium Observations

Four other observations of helium-like vanadium spectra have been reported. Two of these [30,11] were relative measurements to the w line and, as such, can not be compared to absolute measurements of the w line. These relative observations include a study of helium-like vanadium at an EBIT [11] and are the only prior observations of the helium-like resonance lines other than the w line (the x, y and z lines).

Two measurements [31,10] were conducted at a low-inductance vacuum spark plasma and a tokamak plasma respectively. In both cases only the w line was reported. The first study used a double Johann spectrograph and characteristic K lines were used for calibration [31]. The energy of the w was 5.20558(55) keV or a 105 ppm result The second study [10] used a tokamak plasma and claimed an uncertainty of 40 ppm. Close lying Lyman series lines were used for calibration so this was a relative measurement chain assuming one-electron QED. Shorter wavelength calibration lines and helium-like resonances were observed in second order diffraction suggesting the significant systematic shifts discussed above. The third study [11] was a relative measurement to the w line and, as such, can not be compared to absolute measurements.

Dielectronic satellites can affect the precision of measurements. The lithium-like resonances directly concern this research due to their close location to the helium-like resonances and their relatively large electron-impact cross section for

inner shell excitation. We include the estimated influence of satellites in our error budget. Contamination in hot plasmas is often the major limiting uncertainty on the precision of energy measurements [32].

This may be contrasted to the situation in an EBIT where very low satellite contamination can be achieved. A direct comparison between the hot plasma spectrum available from tokomaks at TFR [30] and PLT [10] and our EBIT results demonstrates several key advantages of the EBIT for precision spectroscopy. Firstly, equivalent or better results can be obtained from a very modest experimental facility. The EBIT is essentially a table-top device requiring staffing of only one or two scientists. Secondly, the EBIT spectrum is much cleaner and relatively free of satellite contamination. Thirdly, tokamak spectrum are Doppler-limited at high temperatures and high resolution spectrometers are severely compromised by Doppler broadening and shifts. Finally, we have demonstrated that absolute calibration can be achieved for EBIT spectrum so that the key advantages outlined can be realised ensuring highly accurate spectroscopy.

A selection of experimental measurements across medium Z helium-like resonances is shown in Table 3 and compared with recent theory. The most precise absolute measurement is attributed to Deslattes and co-workers [33] with a 12 ppm measurement of the w transition in argon. Our methodology is similar to that of Deslattes *et al.* in the use of an external X-ray calibration standard lying close to the wavelength of interest. The recoil-ion experimental method used therein also eliminates the need for Doppler corrections and uncertainties in that work as in our EBIT experiment. Argon is at the lower end of the medium Z elements where QED effects are smaller relative to the transition energies. However, this very precise measurement lies below all recent theoretical calculations shown in Table 3.

6 Conclusion

In conclusion, we have made first absolute measurement of helium-like resonances at an EBIT. The results are in accord with Drake [4] and Plante *et al.* [5] and are a 5.7%-8% test of QED contributions. Absolute calibration is achieved by using a spread of characteristic wavelengths to accurately determine the spectrometer dispersion. We have developed the dynamical diffraction theory necessary to evaluate systematic shifts at the precision level required to test QED. Systematic errors associated with the shape and location of the detector in the Johann geometry have been reduced to the level of reference wavelength uncertainty. The benefits of absolute calibration combined with rigorous diffraction theory in precision tests of QED have been demonstrated. The unique spectroscopic advantages of the EBIT have been crucial in the success of these QED investigations, allowing Doppler free and low satellite contamination spectra to be measured.

We acknowledge the assistance of A. Henins, R. D. Deslattes and L. Ratliff during the experiments at NIST. We thank G. W. Drake and K. T. Cheng

for helpful discussions. We acknowledge the support of the Australian Research Council.

References

1. G. W. Series: *The Spectrum of Atomic Hydrogen: Advances* (Utopia, Singapore, 1988)
2. R. Marrus: *Physics of Highly-Ionized Atoms* (Plenum, New York, 1989)
3. G. W. F. Drake: Phys. Rev. A **19**, 1387 (1979)
4. G. W. Drake: Can. J. Phys. **66**, 586 (1988)
5. D. R. Plante, W. R. Johnson, and J. Sapirstein: Phys. Rev. A **49**, 3519 (1994)
6. K. T. Cheng, M. H. Chen, W. R. Johnson, and J. Sapirstein: Phys. Rev. A **50**, 247 (1994); M. H. Chen, K. T. Cheng, and W. R. Johnson: Phys. Rev. A **47**, 3692 (1993)
7. K. T. Cheng and M. H. Chen: Phys. Rev. A **61**, 044503 (2000)
8. P. Indelicato, F. Parente, and R. Marrus: Phys. Rev. A **40**, 3505 (1989); P. Indelicato: Nucl. Instrum. Methods. B **31**, 14 (1988); P. Indelicato, O. Gorceix, and J. P. Desclaux: J.Phys. B **20**, 651 (1987)
9. H. Persson, S. Salomonson, P. Sunnergren, and I. Lindgren: Phys. Rev. Lett. **76**, 204 (1996)
10. P. Beiersdorfer, M. Bitter, S. von Goeler, and K. W. Hill: Phys. Rev. A **40**, 150 (1989)
11. P. Beiersdorfer, M. H. Chen, R. E. Marrs, M. B. Schneider, and R. S. Walling: Phys. Rev. A **44**, 396 (1991)
12. C. T. Chantler, D. J. Paterson, L. T. Hudson, F. G. Serpa, J. D. Gillaspy, and E. Takács: Phys. Rev. A **62**, 042501 (2000)
13. J. D. Gillaspy *et al.*: Physica Scripta T **59**, 392 (1995)
14. J. D. Gillaspy: Physica Scripta T **65**, 168 (1996)
15. B. P. Duval, J. Barth, R. D. Deslattes, A. Henins, and G. G. Luther: Nucl. Instrum. Methods **222**, 274 (1984)
16. A. Henins: Rev. Sci. Instrum. **58**, 1173 (1987)
17. C. T. Chantler, D. J. Paterson, L. T. Hudson, F. G. Serpa, J. D. Gillaspy, and E. Takács: Physica Scripta **T80**, (1999)
18. D. J. Paterson, C. T. Chantler, C. Tran, L. T. Hudson, F. G. Serpa, and R. D. Deslattes: Physica Scripta T**73**, 400 (1997)
19. J. A. Bearden: Rev. Mod. Phys. B **39**, 78 (1967)
20. C. T. Chantler and R. D. Deslattes: Rev. Sci. Instrum. **66**, 5123 (1995)
21. H. F. Beyer and D. Liesen: Nucl. Instrum. Methods A **272**, 895 (1988)
22. P. Beiersdorfer, R. E. Marrs, J. R. Henderson, D. A. Knapp, M. A. Levine, D. B. Platt, M. B. Schneider, D. A. Vogel, and K. L. Wong: Rev. Sci. Instrum. **61**, 2338 (1990)
23. C. T. Chantler: D. Phil. thesis, Oxford University, 1990 (unpublished)
24. C. T. Chantler: J. Appl. Crystallogr. **25**, 674 (1992); C. T. Chantler: J. Appl. Crystallogr. **25**, 698 (1992)
25. J. Schweppe, R. D. Deslattes, T. Mooney, and C. J. Powell: J. Electron Spectrosc. Relat. Phenom. **67**, 463 (1994)
26. D. J. Paterson: Ph.D. thesis, University of Melbourne, 1999 (unpublished)
27. A. H. Gabriel: Mon. Not. R. Astron. Soc. **160**, 99 (1972)

28. W. R. Johnson and G. Soff: Atomic Data and Nuclear Data Tables **33**, 405 (1985); P. J. Mohr, Phys. Rev. A **46**, 4421 (1992)
29. S. MacLaren, P. Beiersdorfer, D. A. Vogel, D. Knapp, R. E. Marrs, K. Wong, and R. Zasadzinki: Phys. Rev. A **45**, 329 (1992)
30. M. H. Achard *et al.*, M. Cornille, J. Dubau, and M. Loulergue TFR Group: Phys. Rev. A **32**, 3000 (1985)
31. E. V. Aglitsky, P. S. Antsiferov, S. L. Mandelstam, A. M. Panin, U. I. Safronova, S. A. Ulitin, and L. A. Vainshtein: Physica Scripta **38**, 136 (1988)
32. E. Träbert: in *The Spectrum of Atomic Hydrogen: Advances* (Utopia, Singapore, 1988), pp. 331–336
33. R. D. Deslattes, H. F. Beyer, and F. Folkmann: J. Phys. B **17**, L687 (1984)